Volume 40
Number 12
December 2025
Pages 3335–3590

JAAS

Journal of Analytical Atomic Spectrometry

rsc.li/jaas

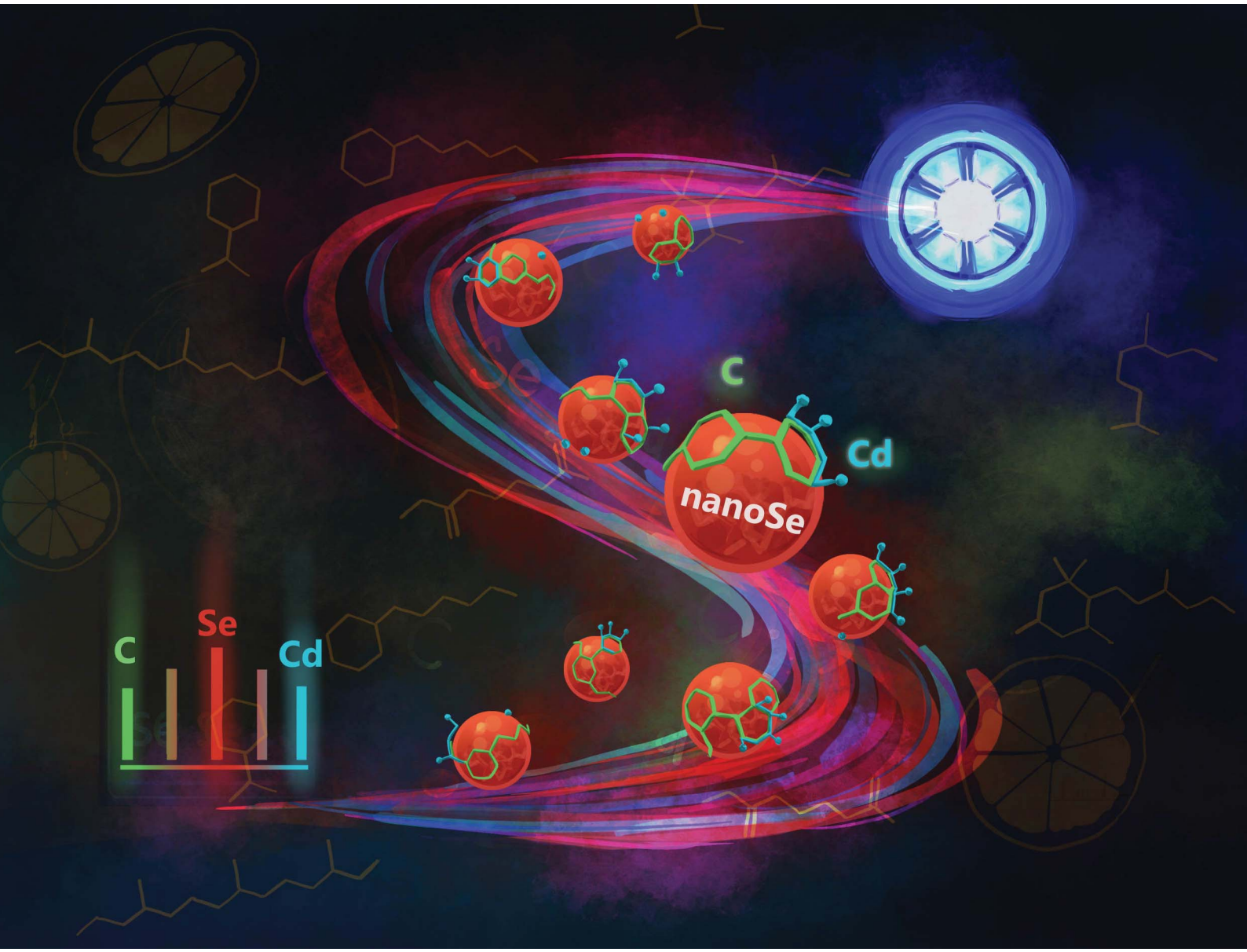

ISSN 0267-9477

ROYAL SOCIETY OF CHEMISTRY

PAPER

Magdalena Borowska and Krzysztof Jankowski
Single particle microwave plasma optical emission spectrometry (SP MWP OES) for selenium nanopowder analysis: from size to elemental composition and surface characteristics

JAAS

PAPER

View Article Online
View Journal | View Issue

Cite this: *J. Anal. At. Spectrom.*, 2025, **40**, 3413

Single particle microwave plasma optical emission spectrometry (SP MWP OES) for selenium nanopowder analysis: from size to elemental composition and surface characteristics

Magdalena Borowska * and Krzysztof Jankowski

Single particle microwave plasma optical emission spectrometry (SP MWP OES) was applied for the characterization of selenium nanopowder synthesized *via* a microwave-assisted green protocol using citrus juice as a reducing and stabilizing agent. The technique enabled real-time, single-particle detection of elemental signals, allowing assessment of particle size distribution and surface composition. The influence of particle size on signal intensity was determined using in-house synthesized quasi-spherical SeNP standards of known sizes. Time-correlated selenium and carbon signals confirmed the presence of surface-bound carbon-containing biomolecules, while co-detection of cadmium indicated potential interactions between SeNPs and cadmium species. These findings highlight the utility of SP MWP OES for probing nanoparticle surface functionalization and compositional variability. Although current calibration focused on spherical SeNPs, further development will address more complex systems. Overall, SP MWP OES proves to be a sensitive and informative tool for the characterization of SeNPs in biologically and environmentally relevant contexts.

Received 29th June 2025
Accepted 4th September 2025

DOI: 10.1039/d5ja00249d

rsc.li/jaas

1 Introduction

Selenium nanoparticles (SeNPs) have emerged as a promising selenium source due to their unique physicochemical properties, including higher bioavailability and lower toxicity compared to conventional Se chemical forms, making SeNPs suitable for biomedical applications such as dietary supplementation.[1] In agriculture, SeNPs enhance the nutraceutical quality of crops and play a role in environmental remediation by reducing cadmium uptake in contaminated soils.[2]

Among various synthesis methods, green synthesis using plant extracts (*e.g.*, citrus) is preferred for its biocompatibility and eco-friendly nature. Microwave-assisted synthesis offers controlled and rapid particle formation, with synthesis parameters significantly influencing nanoparticle size and

Warsaw University of Technology, Faculty of Chemistry, Chair of Analytical Chemistry, Noakowskiego 3, 00-664 Warsaw, Poland. E-mail: magdalena.borowska@pw.edu.pl

Magdalena Borowska

Magdalena Borowska received her PhD in Chemical Sciences from the Warsaw University of Technology in 2021. She has since continued her academic career as an Assistant Professor at WUT. Her PhD thesis focused on developing original analytical methodologies by integrating various sample introduction systems, such as solid-phase microextraction and photochemical vapor generation, with microwave and inductively coupled plasma atomic spectrometry, to investigate the synthesis mechanism of selenium nanoparticles and their characteristics. The Polish Academy of Sciences recognized her thesis as the best doctoral work in the field of analytical spectrometry. Magdalena's work focuses on developing atomic spectrometric techniques such as microwave plasma optical emission spectrometry in single-particle mode (SP-MWP-OES). This innovative approach enables the detection of nanoparticles in powdered form and facilitates the characterization of their interactions with biomolecules and toxic metals, thereby advancing the application of atomic spectroscopy in biological and environmental research. She is particularly interested in microwave plasma, optical emission and mass spectrometry working in conventional and single-particle mode, as well as their hyphenations, connecting analytical chemistry with nanoscience.

morphology.[3] Accurate characterization of SeNPs in terms of size, chemical composition, and surface properties is essential, as these parameters govern their biological activity, stability, and functional performance.

Single particle inductively coupled plasma mass spectrometry (SP ICP MS) is one of the most commonly used methods for characterizing nanomaterials, such as SeNPs, in aqueous media.[4] When tandem mass spectrometry is applied, SP ICP MS/MS offers several analytical advantages,[5,6] including enhanced signal-to-noise ratios and relatively low size detection limits. These features are critical for accurately characterizing the true size distribution and particle number concentration of nanoparticles (NPs) within complex biological and environmental matrices. However, traditional quadrupole-based ICP MS systems are limited by their slow scanning speed and the ability to detect only two isotopes quasi-simultaneously.[7,8] This inherent limitation poses a challenge to comprehensive multi-elemental analysis of nanoparticles using SP ICP MS.[9] In contrast, single particle inductively coupled plasma mass spectrometry with time of flight mass analyzer ICP TOF MS rapidly acquires full elemental mass spectra quasi-simultaneously, making it highly effective for multi-element analysis and transient signal detection.[8,9] This enables the precise characterization of complex nanoparticles, such as core–shell ones.[7,10] Its high-throughput, multiplexed capabilities make it particularly suited for comprehensive analyses in environmental and biological applications. Additionally, the analytical potential of single-particle optical emission spectrometry has also been successfully demonstrated.[11,12]

The dynamic and often unstable nature of nanomaterials in suspension poses a challenge, as they can change properties over time or under different environmental conditions, complicating their characterization.[13,14] Furthermore, the complexity of sample matrices in which nanomaterials are often found, such as biological or environmental systems, can interfere with accurate measurements,[15] necessitating the development of more sophisticated analytical methods. Recently, MWP OES has been introduced for the single particle analysis of inorganic engineered[16] and biologically synthesized nanoparticles.[17] This method is advantageous for examining nanoparticles in powder form at the particle level and distinguishing nanoparticles in mixtures based on elemental composition due to its sensitivity, minimal sample usage, and efficient transport. The technique demonstrates notable detection capabilities when compared to SP ICP MS for various elements.

Currently, a significant challenge in analyzing single particles is size calibration. SP ICP MS is increasingly employed for nanoparticle characterization due to its ability to analyze individual particles. However, accurate calibration, particularly for particle size and distribution, remains a major challenge. This is largely due to limited availability of well-characterized reference materials and the influence of transport efficiency, matrix effects, and instrument-specific limitation.[18,19] For single particle spectrometry, the calibration strategy stems from the Boltzmann equation, and signal intensity is a linear function of the number of atoms in a single particle (particle mass). When assuming spherical shape of the particle, one can calculate the particle equivalent diameter. Current calibration approaches often rely on certified nanoparticle standards (*e.g.*, NIST RM 8013 and 8017),[20,21] though these are insufficient for polydisperse or matrix-rich samples. Matrix effects, including ionization suppression or enhancement, can distort size and concentration data, especially in complex environmental or biological media.[19,22] Additional challenges include detector non-linearity and incomplete particle vaporization, all of which can bias measurements.[23] To address this challenge, a novel approach was employed, marking an advancement in the field. This approach involved using green synthesized size-tunable SeNPs of different diameters to calibrate the single-particle MWP OES technique.

The study aims to evaluate the analytical potential of SP MWP OES for determining the chemical composition and characterizing the surface of SeNPs, synthesized using orange juice as a source of reducing and stabilizing agents. This work also examines the interaction between these SeNPs and cadmium ions to confirm the bioremediation potential of investigated SeNPs. Cadmium is a highly toxic heavy metal that poses severe risks to both human health and the environment, including carcinogenic effects, kidney damage, and soil contamination. SP MWP OES enables the simultaneous detection of the selenium core and surface-associated cadmium within individual particles, providing new insights into the distribution and relationship of these elements that cannot be obtained from bulk measurements alone. Additionally, for the first time, an improved calibration procedure for powder nanomaterials based on nanopowder standards with the use of spherical SeNPs is proposed.

2 Experimental

2.1 Chemicals

Deionized water (18 MΩ cm), produced using a Milli-Q system (Millipore Elix 3, Millipore, Saint-Quentin, France), was utilized in all procedures. The oranges used in this study were obtained from a local grocery store. Selenium dioxide was obtained from Sigma-Aldrich (Steinheim, Germany). Selenium and gold standard solutions, used for SP ICP MS/MS analysis, were prepared from a 1000 mg L^{-1} standard stock solution (Merck, Darmstadt, Germany) by dilution in ultrapure water. Commercial dispersion of gold nanoparticles (AuNPs) with a nominal diameter of 50 nm was purchased from BBI Solutions (Crumlin, UK).

2.2 Microwave-assisted synthesis of selenium nanopowders (SeNPs) with different sizes

SeNPs were synthesized according to Borowska *et al.*[3] In brief, fresh juice was obtained by directly squeezing the orange fruits. The extracted juice was subsequently filtered through a cotton cloth to eliminate pulp and seeds. The filtrate was centrifuged at 5000 rpm for 10 minutes. The supernatant underwent a second round of centrifugation, and the aqueous phase was collected. For the synthesis of SeNPs *via* microwave-assisted techniques, an appropriate volume of juice (30% v/v) was transferred to a Teflon vessel, where the reaction occurred. Subsequently,

a selenite stock solution was added to achieve the desired concentration of the selenium precursor (160 mg L^{-1}) in the reaction mixture. The final volume of the reaction mixture was adjusted to 10 mL with deionized water. The prepared mixture was subsequently exposed to a closed-vessel microwave system, operating at the given power (90 W or 180 W) and duration (5 or 10 minutes), to ensure uniform reaction conditions. The formation of a reddish colloid was indicative of the successful synthesis of SeNPs. Next, the median equivalent diameter of the SeNPs in suspension was measured using SP ICP MS/MS to evaluate variations in nanoparticle characteristics under different synthesis conditions. Following microwave-assisted synthesis, the SeNP suspension was centrifuged at 14 000 rpm for 25 minutes. The resulting pellet was washed twice with distilled water and lyophilized and analyzed using SP MWP OES.

2.3 Cadmium adsorption batch experiments

The synthesis of SeNPs was performed by mixing orange juice (30% v/v) with an appropriate volume of the selenium precursor (400 mg L^{-1}). The reaction mixture was subjected to microwave irradiation for 10 minutes and then to a batch experiment. The SeNPs were incubated with Cd(II) (20 mg L^{-1}) within 8 h under agitation at 150 rpm. Then, the sample was centrifuged (14 000 rpm, 15 minutes). The obtained pellet was then lyophilized and subjected to SP MWP OES analysis.

2.4 Instrumentation

The synthesis of SeNPs was carried out using a MAGNUM II microwave reactor (Ertec, Wrocław, Poland), which was designed for chemical synthesis in a closed-vessel system. The sample incubation was conducted using a magnetic stirrer with heating function, IKA C-MAG HS 7 (China). The separation of the SeNPs resulting from the synthesis was achieved through the utilization of an MPW-352 RH centrifuge (MPW, Poland). Microscopic imaging was performed using a Hitachi SU8230 ultra-high-resolution field-emission scanning electron microscope STEM (Hitachi High-Technologies Corporation, Japan) at 30.0 kV accelerating voltage in bright field STEM mode. Prior to observation, samples were prepared using gold TEM grids coated with a Lacey carbon film, which were immersed in samples' dispersions and dried. Magnifications used were in the range from ×10k to 100k.

The characterization of median diameter of SeNPs in suspension was performed using an Agilent 8900 inductively coupled plasma tandem quadrupole mass spectrometer (ICP MS/MS) equipped with a single nanoparticle application module (Agilent, Tokyo, Japan). The experimental setup involved a concentric nebulizer integrated with a Scott-type double-pass spray chamber, which was utilized for the introduction of the samples. The position of the torch and the nebulizer gas flow were adjusted daily. The RF power was 1550 W, nebulizer gas flow −1.10 L min^{-1}, collision gas flow (hydrogen) −5.0 mL min^{-1}, and sample uptake rate −0.3603 mL min^{-1}. The analyses were performed in time resolved analysis (TRA) mode, monitoring the ^{80}Se isotope. The data were collected within 60 seconds, with a dwell time of 100 μs, and subsequently processed using the SPcal software.[24] The transport efficiency was determined by the use of 50 nm AuNP standards, according to the method described by Pace *et al.* based on the certified particle size.[25]

2.5 SP MWP OES method

SeNPs and their conjugates with Cd were characterized using a laboratory-developed SP MWP OES system, as described in previous studies.[16] The system employed a six-phase rotating field 2.45 GHz helium microwave plasma source (Ertec-Poland, Wrocław, Poland) operating at an optimized power of 300 W. Plasma was generated at atmospheric pressure using helium as a plasma gas. The helium gas flow was set to 700 mL min^{-1} for plasma generation and 90 mL min^{-1} as the carrier gas. The choice of plasma power and plasma gas flow rate was mostly governed by considerations of plasma stability and the excitation potential of the analyte. The custom pneumatic sample introduction system comprised a vertically mounted glass sample chamber and an electrically driven agitator. A precise quantity of SeNPs, measured in milligrams, was meticulously deposited at the bottom of the sample chamber on a frit plate. During measurement, the chamber was mechanically agitated to facilitate sample movement, allowing particles to be drawn by the helium carrier gas through a glass channel and introduced directly into the plasma. This configuration functioned as a comprehensive sample consumption apparatus, with the rate of particle introduction being dictated by the flow rate of the carrier gas. To avoid the memory effect, a dedicated cleaning protocol was implemented. After each measurement, the sample introduction system was purged with filtered air to remove residual airborne nanopowder from the glass chamber and associated components. This was followed by mechanical and solvent-based cleaning where appropriate to dislodge any particles adhering to internal surfaces.

The optical emission from atoms and ions generated upon excitation of nanopowders was collected using a fiber-optic-coupled miniature spectrometer, AvaSpec-2048XL (Avantes, Netherlands) connected *via* an optical fiber positioned within few centimeters of the plasma. The spectrometer operated in TRA mode, covering a spectral range of 200–360 nm. Transient signals were recorded using 20 ms as an integration time per point. The data were obtained using AvaSoft 8.7 software and subsequently processed in Microsoft Excel. A spreadsheet was dedicated to the task of distinguishing nanoparticle signals from background noise, extracting emission intensity distributions, and identifying synchronous emission signals from different particle components. The full spectrum, high resolution, and TRA capabilities of the SP MWP OES system enabled the effective determination of the elemental composition and size distribution of individual selenium nanoparticles and their conjugates.

3 Results and discussion

3.1 Optimization of measurement conditions for single-particle mode

The SP MWP OES technique facilitates comprehensive characterization of dispersed nanomaterials in powder form. Under

optimized conditions, this method allows for both the identification and elemental composition analysis of individual particles. Among the critical parameters influencing data acquisition are nanopowder transport efficiency and signal integration time. To ensure the successful application of the single particle mode, it is essential that nanopowders be introduced into the plasma at a low carrier gas flow rate and with a low sample mass, thereby maintaining a sufficiently small number of particles reaching the plasma at a time. This minimizes particle coincidence events and ensures that the detected signals originate from individual nanoparticles. The carrier gas flow rate plays a critical role in determining the transport efficiency of nanopowder. When helium is used as the carrier gas, the effect of flow rate on the transient signal was evaluated from 50 to 150 mL min^{-1}. Optimal signal representation and temporal resolution were achieved at a flow rate of 90 mL min^{-1}. The gas flow rate strongly depends on the properties of the sample itself, including flowability and bulk density of the nanopowder particles.

To capture representative signals from a single nanoparticle, an integration time ranging between 1 and 50 ms can be applied, with particle transport rates kept below 50 particles per second. An integration time, investigated in the range 10–30 ms, was optimally set to 20 ms adequate temporal resolution, minimizing the occurrence of split particle events, and maintaining sufficient signal intensity for reliable detection.

For a specific elemental constituent of the nanoparticle, the intensity of the signal at a selected emission wavelength provides the basis for converting SP MWP OES data into corresponding nanoparticle size. Subsequently, the raw pulse intensity data are processed to obtain particle size distributions. Additionally, the temporal correlation of emission signals from two distinct elements enables the determination of the elemental composition of individual particles by analyzing the synchronicity of their transient signals as they are introduced into the plasma. The selected wavelengths for monitored analytes were 203.9 (6.32 eV), 247.8 (7.68 eV) and 228.6 (5.41 eV) nm for Se(I), C(I) and Cd(I), respectively.

3.2 Examination of the correlation between the SeNP size and SP MWP OES emission response

SP MWP OES enables the assessment of frequency distributions of signal intensities, which are directly related to particle size distributions. Although the calibration of the optical system for particle sizing is typically performed using pneumatic nebulization of certified powdered reference materials, suitable selenium nanopowder standards are largely unavailable. In the present study, SeNP sizing was conducted by correlating the signal pulses generated when the nanopowder is introduced into the plasma. The SeNP nanopowders used as reference materials had median particle diameters equal to 70, 90 and 126 nm, respectively, depending on the synthesis conditions. The median particle diameter values were determined by SP ICP MS/MS analysis (Fig. S1). Spherical nanoparticles are characterized by their uniform shape, which is critical for precise calibration. This assumption simplifies the data evaluation process, allowing for more straightforward calculations of particle size and size distribution from the raw data and minimizes measurement uncertainty.[20,26]

Different samples were analyzed to determine an average signal intensity for each enabling the correlation between the particle size and signal response as measured by optical emission spectrometry. Typical time scans for selenium signals are presented in Fig. 1. In all cases, the pulse distributions exhibited regularity, with no evidence of signal segregation.

The changes in Se signal intensity distribution displayed in Fig. 1b indicate that with an increase in the median particle diameter, the polydispersity of the material also increases, which is evident from the broadening of the signal intensity distribution for selenium. The size distribution obtained by SP ICP MS further supports this observation (Fig. S1).

Then, the particle size can be evaluated by conversion of signal intensities after applying a detection threshold value to differentiate particles from the background. A calibration graph was then constructed by plotting emission intensity as a function of the cube of the particle diameter (D^3), thus enabling a correlation between the signal response and smaller than 126 nm nanoparticles (Fig. 2). For quantitative particle sizing, the average intensity of pulses measured at a specific emission wavelength can be employed. Assuming a constant particle density and a near-spherical morphology for all nanoparticles (as confirmed by STEM analysis), the particle diameter can be calculated.[16]

The observed nonlinearity in the calibration data occurred most probably due to the less efficient evaporation, atomization or excitation of larger SeNPs within the plasma.[4] Despite the use of helium as a carrier and plasma gas to accelerate particle vaporization, the suppression of the microwave plasma robustness to efficient Se signal generation was observed. The signal produced from SeNPs with a median diameter of 126 nm was more than 30% smaller than expected from the linear regression line based on the signals produced by the 70 and 90 nm SeNP particles. The minimum detectable nanoparticle size in SP MWP OES is determined by the sensitivity of the MWP OES system and its capacity to distinguish particle-derived signals from background noise. For SeNPs, the size detection limit (LOD_{size}) in SP MWP OES was estimated to be 52 nm. For comparison, the $LODs_{size}$ for SeNPs using SP ICP MS have been reported to be as low as 16, 18 and 20 nm, as demonstrated by Freire *et al.*,[27] Jimenez-Lamana *et al.*[4] and Maknun *et al.*,[5] respectively.

Typical particle size distribution plots for SeNP nanopowders with a size of 90 nm obtained by SP MWP OES are displayed in Fig. 3a. The distribution exhibits a unimodal distribution, with a dominant population of particles in the 75–90 nm diameter range, which corresponds to STEM (Fig. 3b) and SP ICP MS/MS analysis (Fig. S1b). Although a strong central tendency is present, the detection of few particles across multiple adjacent size ranges to more than 180 nm demonstrates a degree of heterogeneity in the nanopowder population. The right-skewed tail, with a gradual decrease in particle frequency at higher diameters, also suggests moderate polydispersity.

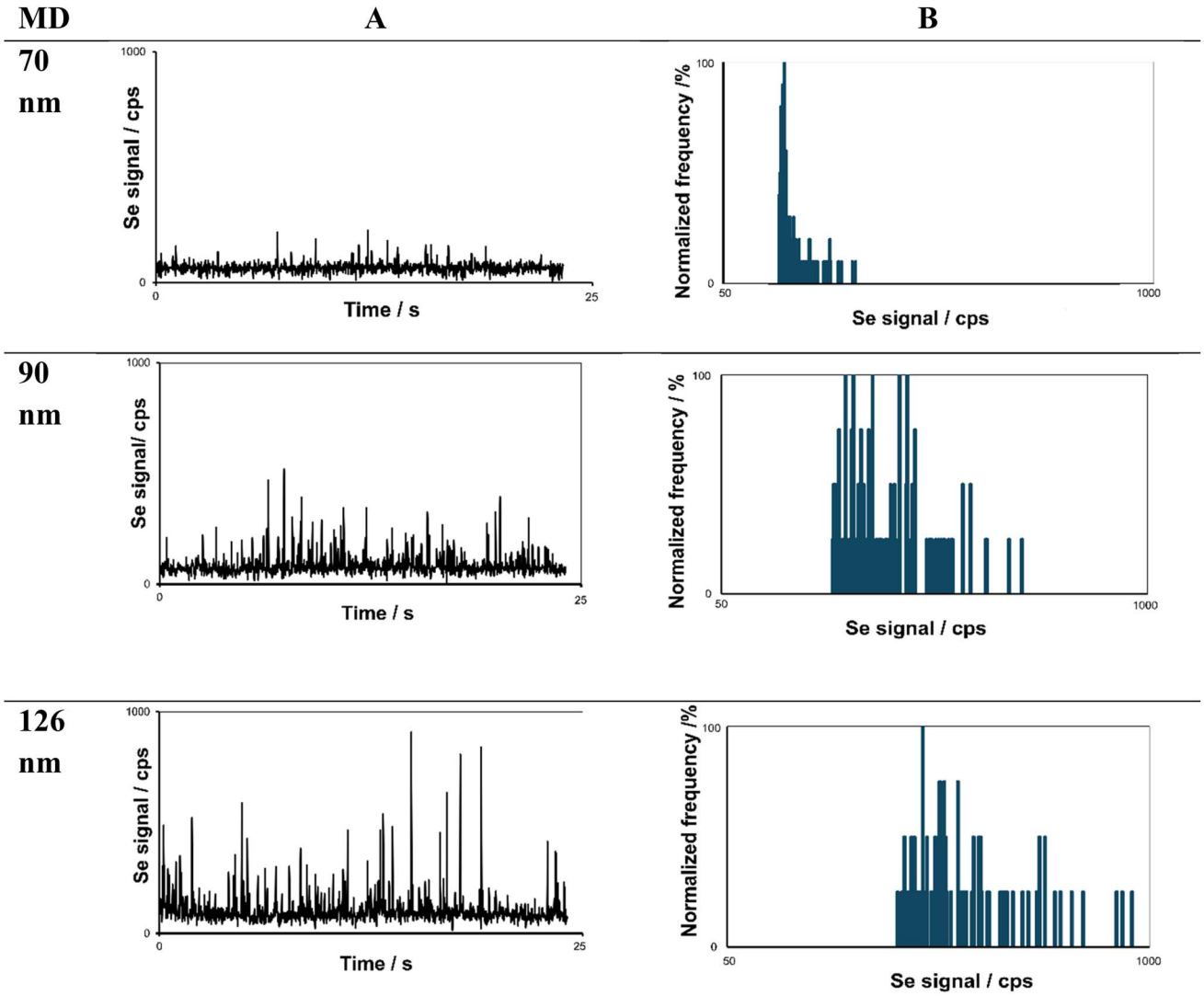

Fig. 1 Time scans (A) and frequency distribution (B) of Se signal intensities for the SeNP sample with median particle diameters of 70 nm, 90 nm, and 126 nm.

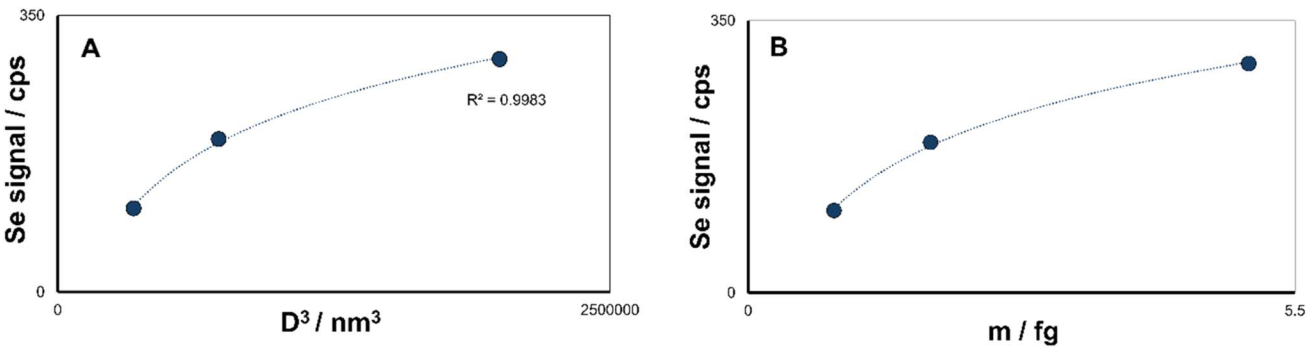

Fig. 2 Se signal as a function of Se D^3 and mass of SeNPs measured by SP MWP OES.

3.3 Examination of chemical composition and surface characteristics of SeNPs

The elemental composition and surface characteristics were also assessed using SP MWP OES. The biomolecules present in citrus juice, which are responsible for surface modification of selenium nanoparticles, contain carbon atoms. Consequently, optical emission from carbon atoms may serve as a useful indicator for the presence of functionalizing/stabilizing groups

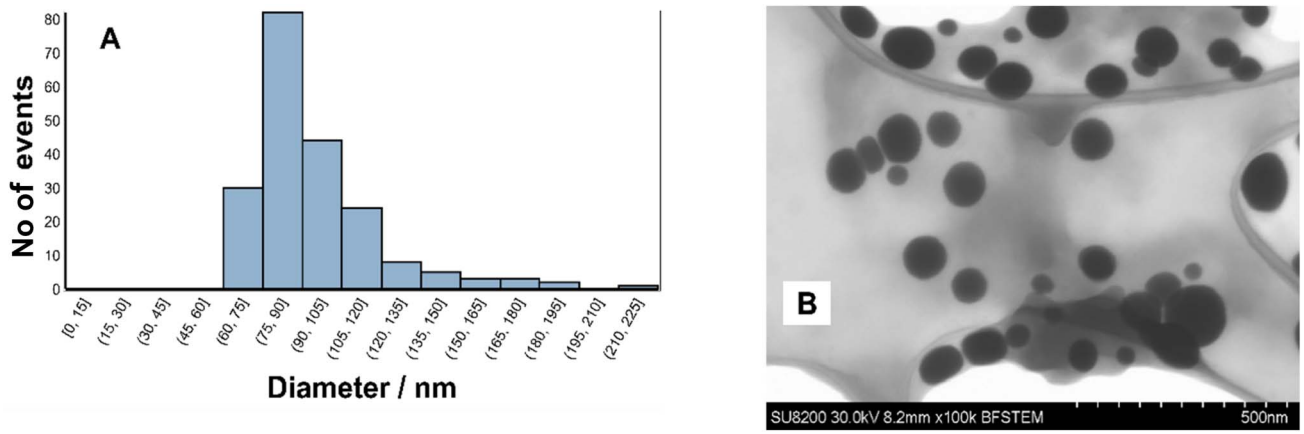

Fig. 3 Particle size distribution for 90 nm SeNPs as obtained by SP MWP OES (A) and microscopic images (B).

onto the NP surface and contribute to the determination of the elemental composition of the SeNPs.

The composition of the nanopowder was assessed through analysis of the synchronicity between Se and C emission pulses. By evaluating the Se/C intensity ratio for all temporally correlated pulses, the particle-by-particle reproducibility of elemental composition across the entire sample can be confirmed (Fig. 4). The regression analysis shown in Fig. 4 yielded a slope of 0.0015, indicating that the Se/C ratio increases by 0.15 for every 100 cps increase in the Se signal. This proportionality reflects the consistent relationship between the selenium signal intensity and particle composition, supporting the robustness of the measurement approach. The high R^2 value of 0.9541 confirms that the Se/C ratio is strongly correlated with Se signal intensity across the measured particle size range. The observed trend indicates that the Se/C ratio increases with increasing selenium signal intensity, suggesting a decrease in relative carbon content per nanoparticle as selenium content and thus particle size increases. This implies that larger SeNPs exhibit a lower degree of surface functionalization with carbon-containing compounds relative to their core selenium content. The finding aligns with the understanding that as the nanoparticle size increases, the surface-area-to-volume ratio decreases. This trend also suggests a non-uniform distribution of carbon-based functional groups across the nanopowder population, with smaller particles being more richly functionalized per selenium atom. Such a pattern is consistent with functionalization mechanisms driven by surface interactions, which are inherently more effective in smaller nanoparticles due to their higher surface area of interaction per mass unit compared with bigger particles.[28,29]

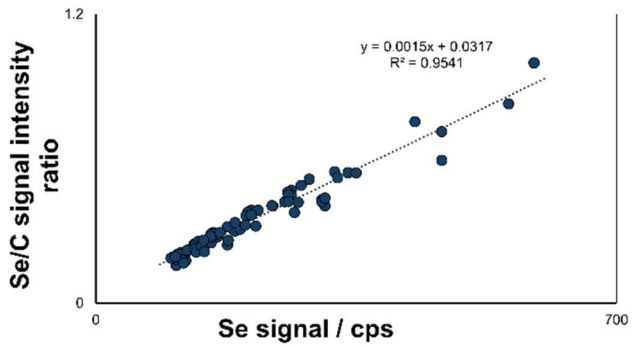

Fig. 4 Relationship between the Se/C signal intensity ratio and the selenium signal intensity recorded for the sample with median particle diameter equal to 126 nm.

The relationship between Se and C emission intensities was examined for SeNPs of varying diameters of 70 nm, 90 nm, and 126 nm to evaluate the influence of particle size on surface functionalization by carbon-containing organic molecules. Two to three different samples were analyzed for each one. The results, expressed as correlation plots with respective regression models and coefficients of determination, are presented in Fig. 5. A temporal correlation plot of Se and C signals for all particles within the selenium nanoparticle sample demonstrates that the emission signals are synchronous, exhibit strong correlation for smaller NPs, and display a clear dependence on particle size with variation of coating thickness for different SeNP sizes. In the case of spherical particles exhibiting surface ideal surface coating, the correlation between the coating components and the base material typically follows a trend that approximates a curve proportional to the base particle diameter raised to the power of 2/3. In the case of investigated nanopowders, the relationships have a logarithmic relationship. These results indicate that each SeNP is coated with carbon-containing molecules present in orange juice, and that the extent of surface functionalization is significantly influenced by the nanoparticle size.

Based on the signal correlations presented in Fig. 5 for SeNPs of varying diameters, it was observed that with increasing nanoparticle size, both the selenium signal intensities and their range increase, ranging from approximately 80 cps for the smallest diameter to around 600 cps for the largest nanoparticle size. These findings confirm a higher degree of polydispersity for SeNP nanopowders with larger particles. For SeNPs with a nominal diameter of 70 nm, a moderate linear correlation was observed between selenium and carbon signals, with an R^2

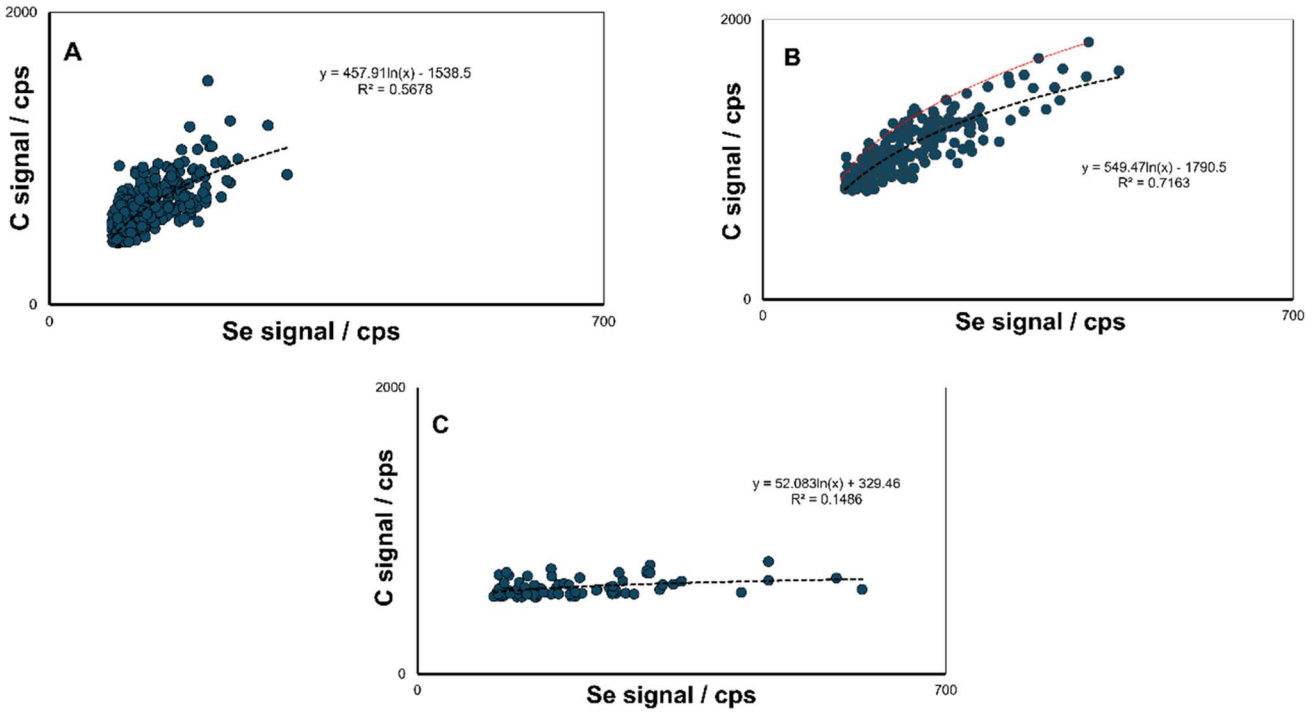

Fig. 5 Correlation between Se and C events for SeNP nanopowders with median particle diameter equal to (a) 70 nm, (b) 90 nm, and (c) 126 nm.

value of 0.5678. This suggests a variable but positive relationship between the core selenium content and the amount of associated carbon species, indicative of partial or non-uniform surface coverage by functionalizing molecules. As shown in Fig. 5, variations in the fitting coefficient may also arise from differences in the variability range of the Se signal. In the case of monodisperse particles, the reduced signal dispersion typically leads to weaker correlation strength.

In the case of 90 nm SeNPs, the Se–C correlation exhibited the highest degree of linearity among the three size groups, with an R^2 value of 0.7163. The elevated correlation coefficient may be attributed to the broader range of recorded Se signal intensities, indicative of increased nanopowder dispersity. This strong positive correlation reflects a more consistent and proportional distribution of carbon-based functional groups on the nanoparticle surface relative to selenium content. The data suggest that SeNPs of this size may represent an optimal configuration for uniform functionalization, possibly due to a favorable balance between surface area availability and ligand accessibility. The results indicate that the experimentally observed coating thickness exhibits considerable variation across the entire particle population (red line in Fig. 5b). This effect may be attributed to the multilayer adsorption of oppositely charged biomolecules, which promotes the formation of a second random layer on the nanoparticle surface as in the case of protein. On the other hand, this may also result from the coexistence of particles functionalized with different biomolecules. However, further research is required to confirm this hypothesis.

Conversely, the SeNPs with a diameter of 126 nm showed a markedly different trend. Here, the Se–C relationship exhibited a notably low R^2 value of 0.1486. This weak correlation indicates that the carbon signal intensity remains largely invariant across a wide range of selenium intensities, implying poor or inconsistent functionalization. In the case of carbon emission signals, it can be noted that for SeNPs with the largest diameter, the intensities are significantly lower compared to the other samples. The emission intensity of the coating component is associated with the surface area of the nanoparticle, whereas the intensity corresponding to the core particle component reflects its total volume. This suggests that as the particle size increases, the quantity of organic functionalizing agents on the particle surface decreases, which is consistent with the trend observed in the plot of the Se/C intensity ratio *versus* selenium intensity. The diminished surface-area-to-volume ratio in larger nanoparticles likely limits the number of accessible binding sites for organic molecules. Additionally, analytical constraints such as incomplete transport, atomization, or excitation of larger particles in the plasma may further contribute to the reduced carbon signal response.

These results demonstrate a size-dependent trend in SeNP surface functionalization, with the strongest selenium–carbon signal correlation observed for 90 nm particles. Thus, nanoparticle size plays a critical role in determining the efficiency and uniformity of organic surface modification, which is essential for applications requiring controlled surface chemistry.

3.4 Examination of Cd ion – SeNP interaction

Raw time-resolved data of the analyzed sample expressed as intensity *versus* time were processed to determine the particle size distribution of SeNPs after interaction with cadmium.

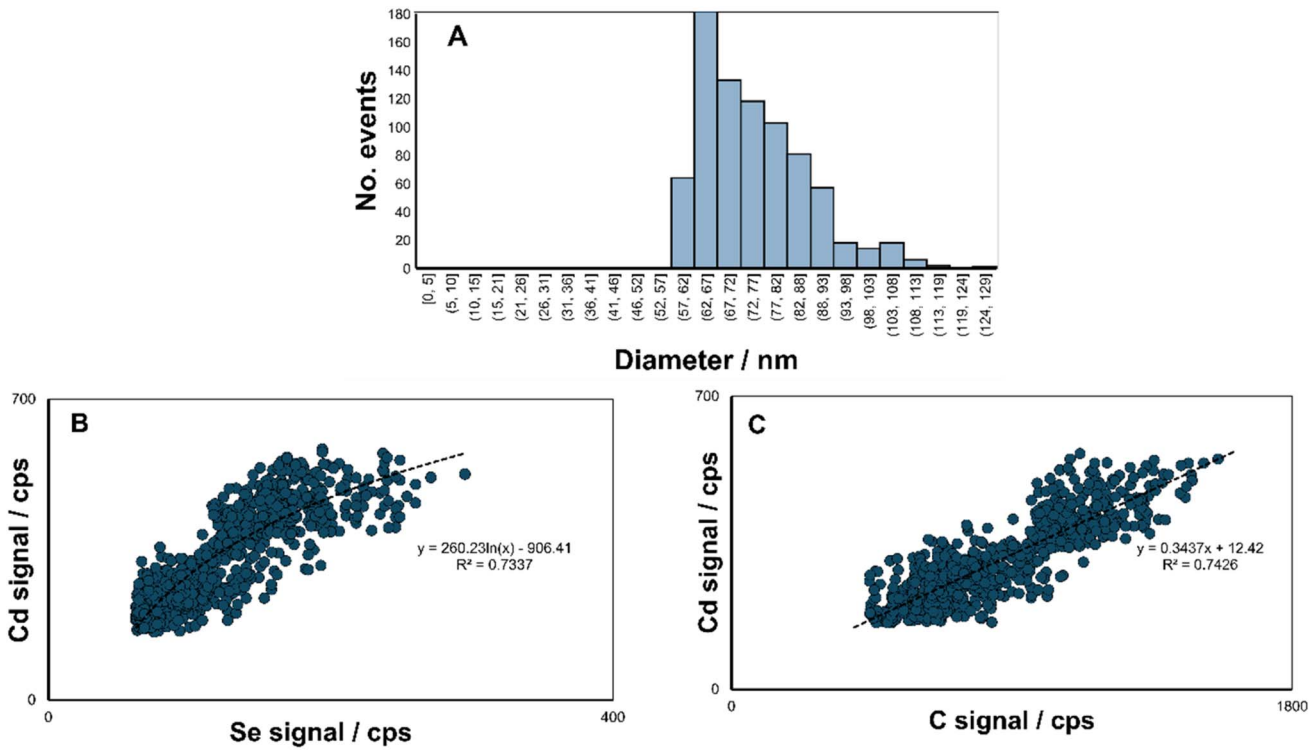

Fig. 6 Particle size distribution for SeNPs after cadmium adsorption (A), correlation plot between Se–Cd (B) and C–Cd (C) events for SeNP nanopowders.

Occasional high-intensity pulses, indicative of particle agglomerates, were also observed. The acquired data were imported into a custom-developed computational worksheet, wherein a detection threshold was applied to discriminate particle signals from background noise. The filtered intensity values were then converted into particle diameters based on previously performed calibration, yielding the final particle size distribution (Fig. 6a).

The particle size distribution shows a predominant population within the range of about 60–90 nm. Only a minor fraction of particles exceeded 100 nm, suggesting that the presence of larger aggregates is negligible. Collectively, these findings indicate that the sample possesses a relatively narrow size distribution.

The correlation analysis of selenium, cadmium, and carbon signals revealed the presence of cadmium in the composition of the nanopowders following the sorption process.

Different interaction profiles were observed between selenium and cadmium compared to those between carbon and cadmium. The correlation between selenium and cadmium exhibited a logarithmic relationship (Fig. 6b). The amount of cadmium increases with increasing particle size, corresponding to higher signal intensity. It suggests that nanoparticles are uniformly coated with cadmium. The moderate R^2 value reflects variability, potentially due to heterogeneity in surface composition or functional group distribution. Such findings highlight not only the uniformity of the SeNP size but also their capacity to interact with toxic metal ions, underscoring their potential application in environmental remediation strategies.

However, Fig. 6c shows a linear relationship between cadmium and carbon. The linear relationship between carbon and cadmium signals points to a direct and proportional interaction, likely due to cadmium binding directly with carbon-containing surface functional groups. The correlation indicates a more consistent and predictable interaction compared to the Se *vs.* Cd correlation, supporting the role of surface-bound organic compounds rich in carbon, as primary binding sites for cadmium. This suggests that cadmium does not bind directly to selenium atoms but rather interacts through organic molecules present on the nanoparticle surface. These functional groups, often derived from biological synthesis agents, facilitate cadmium sorption. These interactions probably occur *via* electrostatic attraction, complexation, or chelation mechanisms involving functional groups capable of binding metals, such as amino or carboxyl groups originating from amino acids. The presence of these groups was confirmed in studies of compounds involved in the synthesis of SeNPs.[3] The data suggest a mechanistic distinction in how cadmium interacts within the SeNP system. This differential interaction is important for understanding metal adsorption behavior in functionalized nanoparticles and has implications for their application in environmental and biological fields.

4 Conclusion

SP MWP OES has demonstrated strong potential as a powerful analytical technique for investigating the elemental composition and surface characteristics of SeNPs. The method enables

sensitive, single particle level detection of elemental signals, allowing for the differentiation of particle subpopulations based on compositional variability. Moreover, the correlation between selenium and co-associated elements such as carbon and cadmium provides valuable insights into surface interactions and the presence of organic or inorganic surface coatings. The ability of SP MWP OES to detect variations in carbon signal intensity further supports its utility in assessing surface bound molecular species, offering indirect but meaningful evidence of functionalization or environmental modification of SeNP surfaces. These capabilities highlight SP MWP OES as a feasible and informative approach for both core composition analysis and surface characterization, particularly for environmentally and biologically relevant nanoparticles such as SeNPs, which can be considered promising candidates for cadmium remediation. To ensure accurate interpretation of signal intensities, calibration was performed using SeNP standards of different sizes, allowing estimation of particle size-dependent responses and elemental sensitivities. SeNPs synthesized with the use of biomolecules proved to be attractive as potential standards for SP MWP OES calibration since they can be easily produced as single-element particles of regular spherical or quasi-spherical shape and can be further stored and utilized as stable non-aggregated nanopowder materials. However, this calibration work is ongoing and will be further extended to include more complex nanopowder samples with diverse shapes and size distributions, which are expected to influence signal behavior and detection efficiency. Expanding the calibration framework will enhance the quantitative capabilities of SP MWP OES and support its broader application in nanopowder research.

Author contributions

MB: conceptualization, methodology, investigation, validation, visualization, project administration, funding acquisition, formal analysis, writing – original draft, writing – review & editing; KJ: writing – review & editing.

Conflicts of interest

There are no conflicts to declare.

Data availability

The data supporting the findings of this study are included in the main article and SI material. Additional raw data files are available upon reasonable request. Supplementary information is available. See DOI: **https://doi.org/10.1039/d5ja00249d**.

Acknowledgements

The financial support from the Warsaw University of Technology within the Excellence Initiative: Research University (IDUB) programme (Young PW II) and NCHEM3 grant is acknowledged. The authors acknowledge Maciej Trzaskowski and the Centre for Advanced Materials and Technologies CEZAMAT PW (Warsaw University of Technology) for the help in electron microscopy analysis.

References

1 B. Hosnedlova, M. Kepinska, S. Skalickova, C. Fernandez, B. Ruttkay-Nedecky, Q. Peng, M. Baron, M. Melcova, R. Opatrilova, J. Zidkova, G. Bjørklund, J. Sochor and R. Kizek, *Int. J. Nanomed.*, 2018, **13**, 2107–2128, DOI: **10.2147/IJN.S157541**.

2 B. Cheng, J. Zhang, C. Wang, J. Li, F. Chen, X. Cao, L. Yue and Z. Wang, *Chemosphere*, 2023, **344**, 140320, DOI: **10.1016/j.chemosphere.2023.140320**.

3 M. Borowska, J. Pszczoła, K. Pawlak, L. Ruzik, J. N. Ombugadu, M. Trzaskowski and K. Jankowski, *Colloids Surf., A*, 2025, **725**, 137516, DOI: **10.1016/j.colsurfa.2025.137516**.

4 J. Jiménez-Lamana, I. Abad-Álvaro, K. Bierla, F. Laborda, J. Szpunar and R. Lobinski, *J. Anal. At. Spectrom.*, 2018, **33**, 452–460, DOI: **10.1039/C7JA00378A**.

5 L. Maknun, J. Sumranjit and A. Siripinyanond, *RSC Adv.*, 2020, **10**, 6423–6435, DOI: **10.1039/C9RA07120B**.

6 A. B. S. da Silva and M. A. Z. Arruda, *Spectrochim. Acta, Part B*, 2023, **203**, 106663, DOI: **10.1016/j.sab.2023.106663**.

7 S. Naasz, S. Weigel, O. Borovinskaya, A. Serva, C. Cascio, A. K. Undas, F. C. Simeone, H. J. P. Marvina and R. J. B. Peters, *J. Anal. At. Spectrom.*, 2018, **33**, 835–845, DOI: **10.1039/C7JA00399D**.

8 X. Tian, H. Jiang, L. Hu, M. Wang, W. Cui, J. Shi, G. Liu, Y. Yin, Y. Cai and G. Jiang, *TrAC, Trends Anal. Chem.*, 2022, **157**, 116746, DOI: **10.1016/j.trac.2022.116746**.

9 F. Laborda, I. Abad-Álvaro, M. S. Jiménez and E. Bolea, *Spectrochim. Acta, Part B*, 2023, **199**, 106570, DOI: **10.1016/j.sab.2022.106570**.

10 L. Hendriks, A. Gundlach-Graham and D. Günther, *J. Anal. At. Spectrom.*, 2019, **34**, 1900–1909, DOI: **10.1039/C9JA00186G**.

11 Y. Y. Su, Z. M. Li, W. L. Wang, J. Xu, W. Wang, X. Z. Li and Z. Yu, *J. Anal. At. Spectrom.*, 2017, **32**, 2469–2475, DOI: **10.1039/c7ja00221a**.

12 T. N. Kröger, S. Wiemers-Meyer, P. Harte, M. Winter and S. Nowak, *Anal. Chem.*, 2021, **93**, 7532–7539, DOI: **10.1021/acs.analchem.1c01283**.

13 P. Pusuwan and A. Siripinyanond, *Microchem. J.*, 2024, **196**, 109705, DOI: **10.1016/j.microc.2023.109705**.

14 D. M. Mitrano, J. F. Ranville, A. Bednar, K. Kazor, A. S. Heringd and C. P. Higgins, *Environ. Sci.: Nano*, 2014, **1**, 248–259, DOI: **10.1039/C3EN00108C**.

15 Y. U. Hachenberger, D. Rosenkranz, C. Kromer, B. C. Krause, N. Dreiack, F. L. Kriegel, E. Koz'menko, H. Jungnickel, J. Tentschert, F. S. Bierkandt, P. Laux, U. Panne and A. Luch, *Nanomaterials*, 2023, **13**, 1–18, DOI: **10.3390/nano13050922**.

16 M. Borowska, J. Giersz and K. Jankowski, *Anal. Chim. Acta*, 2019, **1089**, 25–31, DOI: **10.1016/j.aca.2019.08.053**.

17 M. Borowska, E. Pawlik and K. Jankowski, *Monatsh. Chem.*, 2020, **151**, 1283–1290, DOI: **10.1007/s00706-020-02663-w**.

18 A. N. Geraldes, M. A. Hortellani, M. E. C. M. Rostelato and J. E. S. Sarkis, *J. Braz. Chem. Soc.*, 2025, **36**, 1–8, DOI: **10.21577/0103-5053.20250011**.
19 F. Laborda, A. C. Gimenez-Ingalaturre and E. Bolea, *Compr. Anal. Chem.*, 2021, 35–67, DOI: **10.1016/BS.COAC.2021.02.012**.
20 J. Liu, K. E. Murphy, M. R. Winchester and V. A. Hackley, *Anal. Bioanal. Chem.*, 2017, **409**, 6027–6039, DOI: **10.1007/S00216-017-0530-4**.
21 A. R. M. Bustos, K. E. Murphy and M. R. Winchester, *Anal. Chem.*, 2022, **94**, 3091–3102, DOI: **10.1021/acs.analchem.1c04140**.
22 Y. Huang, J. T.-S. Lum and K. S.-Y. Leung, *J. Anal. At. Spectrom.*, 2020, **35**, 2148–2155, DOI: **10.1039/D0JA00180E**.
23 W.-W. Lee and W.-T. Chan, *J. Anal. At. Spectrom.*, 2015, **30**, 1245–1254, DOI: **10.1039/C4JA00408F**.
24 T. E. Lockwood, R. Gonzalez de Vega and D. Clases, *J. Anal. At. Spectrom.*, 2021, **36**, 2536–2544, DOI: **10.1039/D1JA00297J**.
25 H. E. Pace, N. J. Rogers, C. Jarolimek, V. A. Coleman, C. P. Higgins and J. F. Ranville, *Anal. Chem.*, 2011, **83**, 9361–9369, DOI: **10.1021/ac201952t**.
26 S. Yamashita, S. I. Miyashita and T. Hirata, *Nanomaterials*, 2023, **13**, 1–12, DOI: **10.3390/nano13131958**.
27 B. M. Freire, Y. T. Cavalcanti, C. N. Lange, J. C. Pieretti, R. M. Pereira, M. C. Gonçalves, G. Nakazato, A. B. Seabra and B. L. Batista, *Nanotechnology*, 2022, **33**, 355702, DOI: **10.1088/1361-6528/ac723e**.
28 K. Wieszczycka, K. Staszak, M. J. Woźniak-Budych, J. Litowczenko, B. M. Maciejewska and S. Jurga, *Coord. Chem. Rev.*, 2021, **436**, 213846, DOI: **10.1016/j.ccr.2021.213846**.
29 A. Yusuf, A. R. Z. Almotairy, H. Henidi, O. Y. Alshehri and M. S. Aldughaim, *Polymers*, 2023, **15**, 1–26, DOI: **10.3390/polym15071596**.